INSTITUTE OF PHYSICS PUBLISHING JOURNAL OF PHYSICS: CONDENSED MATTER

J. Phys.: Condens. Matter **18** (2006) S969–S978 doi:10.1088/0953-8984/18/25/S05

Nonhydrostatic compression of gold powder to 60 GPa in a diamond anvil cell: estimation of compressive strength from x-ray diffraction data

A K Singh[1,5], H P Liermann[2], S K Saxena[3], H K Mao[4] and S Usha Devi[1]

[1] Materials Science Division, National Aerospace Laboratories, Bangalore 560 017, India
[2] HPCAT, Advanced Photon Source, Argonne National Laboratory, Argonne, IL 60439-4803, USA
[3] Center for Study of Matter at Extreme Conditions (CeSMEC), Florida International University, Miami, FL 33199, USA
[4] Geophysical Laboratory and Center for High Pressure Research, Carnegie Institution of Washington, Washington DC 20015, USA

E-mail: aksingh@css.nal.res.in

Received 26 November 2005, in final form 23 March 2006
Published 8 June 2006
Online at stacks.iop.org/JPhysCM/18/S969

Abstract

Two gold powder samples, one with average crystallite size of ≈30 nm (n-Au) and another with ≈120 nm (c-Au), were compressed under nonhydrostatic conditions in a diamond anvil cell to different pressures up to ≈60 GPa and the x-ray diffraction patterns recorded. The difference between the axial and radial stress components (a measure of the compressive strength) was estimated from the shifts of the diffraction lines. The maximum micro-stress in the crystallites (another measure of the compressive strength) and grain size (crystallite size) were obtained from analysis of the line-width data. The strengths obtained by the two methods agreed well and increased with increasing pressure. Over the entire pressure range, the strength of n-Au was found to be significantly higher than that of c-Au. The grain sizes of both n-Au and c-Au decreased under pressure. This decrease was much larger than expected from the compressibility effect and was found to be reversible. An equation derived from the dislocation theory that predicts the dependence of strength on the grain size and the shear modulus was used to interpret the strength data. The strength derived from the published grain size versus hardness data agreed well with the present results.

1. Introduction

Compression of a solid without a pressure-transmitting medium in a diamond anvil cell (DAC) results in a nonhydrostatic stress state. The macroscopic stress state at the centre of the

[5] Author to whom any correspondence should be addressed.

sample is axially symmetric about the load axis of the DAC and the difference between the axial and radial stress components (t) is taken as a measure of the compressive strength of the sample material at a pressure that equals the mean normal stress [1]. It is possible to derive t and the single-crystal elastic constants by analysing the high-pressure diffraction patterns using the approach developed in earlier works [2–9]. The experimental studies [10–30] provide examples of the in-depth information that such analyses offer. The maximum micro-stress $2p_{\max}$ [31] (another measure of strength) and the grain size (crystallite size) can be derived from the diffraction line-width data (e.g. [32–35]). The estimation of $2p_{\max}$ from high-pressure diffraction data has received limited attention [36–39]. The possibility of the grain (crystallite) size changing under nonhydrostatic compression and influencing the strength has long been ignored. A recent study [40] on magnesium oxide reported the reduction in grain size on compression in a DAC and the resulting increase in t. Similar observations were reported subsequently on magnesium oxide compressed in a multi-anvil device [41]. Though consideration of the yield criterion [1] suggests that t is a measure of compressive yield strength, this parameter has not been compared in the past with the strength obtained by another method. Further, both t and $2p_{\max}$ have been taken as measures of compressive strength and their equivalence implicitly assumed. In the present study, we compressed to ≈60 GPa two samples of gold powder with average crystallite sizes of ≈30 nm (n-Au) and ≈120 nm (c-Au) in a DAC and recorded the x-ray diffraction patterns. The t-values at different pressures were derived from the line shift data, and $2p_{\max}$ and the grain size from the line width data. The results were analysed using a dislocation theory based equation that predicts the pressure (through the shear modulus) and grain-size dependences of strength. The values of t and $2p_{\max}$ were compared. The grain-size dependence of strength derived from $2p_{\max}$ was compared with the strength derived from the published one-atmosphere grain size versus hardness data [42] in order to ascertain that the parameters $2p_{\max}$ and t do represent compressive strength.

2. Experimental details

The powder samples of nanocrystalline gold (n-Au) from Nanomat Inc, Pennsylvania, USA and coarser-grained gold (c-Au) of high purity from Goodfellow Corporation, Pennsylvania, USA were used in the present study. The crystallite size and the micro-strains in the starting samples were determined using high-quality diffraction patterns taken with a Philips diffractometer using Cu Kα radiation. In a typical high-pressure diffraction experiment, the powder sample contained in a stainless-steel gasket, 400 μm thick with a 40 μm thick indented region and a hole diameter of 125 μm, was compressed in a DAC. No pressure-transmitting medium was used to maximize the nonhydrostatic stress state. The high-pressure diffraction experiments were conducted at the HPCAT synchrotron beam line at the Advanced Photon Source (APS), Chicago. The experiments on c-Au and n-Au were conducted at different times and the available primary x-ray beam wavelength λ was 0.038 51 nm for n-Au samples and 0.040 84 nm for c-Au samples. The beam size in both sets of experiments was 20 μm. The x-ray diffraction patterns were recorded on an image plate using the conventional DAC geometry, wherein the primary x-ray beam is parallel to the load axis. Typical diffraction patterns are shown in figure 1. The positions and widths (full width at half maximum, FWHM) of the diffraction peaks were obtained by fitting a four-parameter pseudo-Voigt function to each peak.

3. Method of data analysis

The sample, on compression between the anvils, undergoes considerable plastic deformation before the complex equilibrium stress state is established. The macro-stress component causes

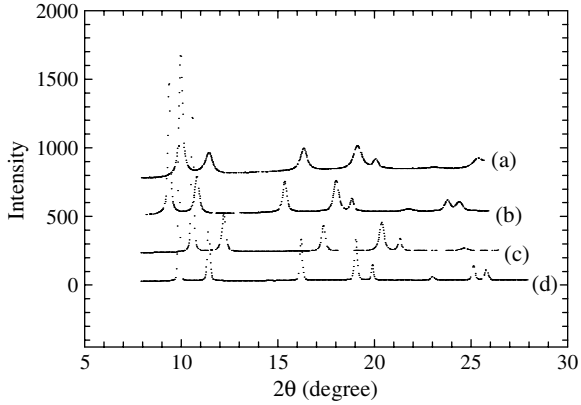

Figure 1. Diffraction patterns (a) and (b) are from n-Au at 55 GPa and 3.3 GPa, respectively; $\lambda = 0.038\,51$ nm. (c) and (d) are from c-Au at 58.8 GPa and 0.2 GPa, respectively; $\lambda = 0.040\,84$ nm.

the shift of the diffraction lines, while the micro-stresses cause line broadening. The macro-stresses at the centre of the sample are considerably simpler to describe, because of the axial symmetry that exists about the load axis of the DAC. The difference between the axial and radial stress components (t) has been suggested as a measure of the yield strength of the sample material [1]. The detailed analyses given earlier [3, 6, 8] show that the lattice parameter $a_m(hkl)$ of the cubic system, computed from the measured line positions $2\theta_{hkl}$ taken with the conventional DAC geometry, is given by the following relation:

$$a_m(hkl) = M_0 + M_1[3(1 - 3\sin^2\theta_{hkl})\Gamma(hkl)], \tag{1}$$

where,

$$\Gamma(hkl) = (h^2k^2 + k^2l^2 + l^2h^2)/(h^2 + k^2 + l^2)^2. \tag{2}$$

M_0 and M_1 are constants at a given pressure and are functions of t, the lattice parameter, and single-crystal elastic compliances S_{ij}, all the quantities being at equivalent hydrostatic pressure that equals the mean normal stress. At a given pressure, the plot of $a_m(hkl)$ against $3(1 - 3\sin^2\theta_{hkl})\Gamma(hkl)$, referred to as the gamma-plot, is a straight line. The parameters M_0 and M_1 can be determined from such plots. Knowing S_{ij} at the relevant pressure, t can be computed from the relation,

$$t = -3M_1/\alpha M_0(S_{11} - S_{12} - S_{44}/2). \tag{3}$$

The details of this method are discussed in an earlier publication [8]. The term α decides the relative weights of the iso-stress and iso-strain conditions. In many studies [25, 26], the assumption of $\alpha = 1$ under high-pressure conditions is found to yield satisfactory results. However, the elastic anisotropy of gold [21] determined from the high-pressure x-ray diffraction data was found to agree well with the results from ultrasonic velocity measurement if $\alpha \cong 0.5$ was assumed. Following this result, we assume $\alpha = 0.5$ in the present analysis. The assumptions underlying the lattice strain equations are discussed later in the paper.

Stokes *et al* [31] proposed a model for the micro-stresses in the deformed crystallites and discussed its effect on the line broadening. We extend this model for the high-pressure case by assuming that the stresses in the crystallites occur with equal probability between a minimum and a maximum and identify the difference between the two with the maximum stress $2p_{\max}$ in the theory of Stokes *et al* [31]. The standard equation [32] describing the grain-size and

micro-strain dependences of the line width was modified by Singh [28, 40] for the analysis of high-pressure diffraction data as follows:

$$(2w_{hkl}\cos\theta_{hkl})^2 = (\lambda/d)^2 + [4p_{\max}/E_{hkl}]^2\sin^2\theta_{hkl}. \tag{4}$$

$2w_{hkl}$ is the FWHM on 2θ-scale. E_{hkl} is the single-crystal Young's modulus in the direction $[hkl]$ and d is the crystallite (grain) size. Equation (4) is strictly valid for Gaussian profiles.

4. Results and discussion

The lattice strain theories [2–8] for the analysis of the diffraction data under nonhydrostatic compression were derived using an averaging procedure that assumed random orientation of the crystallites in the polycrystalline sample. This assumption is certainly not valid, as the sample undergoes considerable plastic deformation on compression, resulting in texture (preferred orientation). Though the theories with this underlying assumption were successful in explaining almost all the features observed in the diffraction data, quantitative deviations were observed in the single-crystal elastic moduli, particularly in the case of the hexagonal system [43]. The presence of texture was suspected as the reason [44]. The studies on MgO [26] and epsilon-iron [29] used elasto-plastic modelling to solve the equations in a self-consistent manner. It has been shown [45] that t for epsilon-iron determined using earlier theory is in excellent agreement with those obtained using elasto-plastic modelling [29]. Similar agreement was observed for the case of MgO [40]. The solution of t from the lattice strain equations is robust and is not affected greatly by this assumption or by the neglect of elasto-plastic effects.

The strains measured from the shift of the diffraction lines and the stresses computed as a result are essentially elastic in nature, as supported by the fact that the strains vanish on decompressing the sample to ambient pressure. This justified the assumption that the stress state was described adequately by a state that lay between the Voigt and Reuss limits. The choice of α between 0 and 1 was therefore used in the development of the lattice strain theories [2–8]. A recent study [46] suggested that $\alpha > 1$ in the plastic deformation regime. An article in this volume [47] discusses the elasto-plastic model. As discussed following equation (3), $\alpha = 0.5$ is used in the present analysis. Since t is invariably small, linear elasticity was used to derive the equations that connect strain with t.

The grain size and the micro-strains in the starting powder samples were determined by analysing the FWHM determined from diffractometer records using the simplified approach suggested by Langford [31]. This gave 120 ± 15 nm and 33 ± 3 nm for the d of c-Au and n-Au, respectively. The errors indicated are the standard errors. The micro-strains were 0.8×10^{-3} and 1.8×10^{-3} for c-Au and n-Au, respectively. Langford's method is based on the assumption that the diffraction profiles are Gaussian. In general, the profiles contain a significant contribution from the Lorentzian term. For this reason, a more rigorous method based on integral widths [34] was also used to determine d and micro-strains. The results from the two methods did not differ significantly. The quality of high-pressure diffraction line profiles was not high enough to permit the use of more rigorous methods [33].

Figure 2 shows typical gamma-plots. The single-crystal elastic compliances at high pressures required in equation (3) were estimated using one-atmosphere values of single-crystal elastic moduli and their pressure derivatives [48] in the Birch equations [49]. Implicit in the present analysis is the assumption that the elastic moduli of the crystalline region do not change on reducing the grain size down to a few tens of nanometres. This assumption is supported by the results of many studies. For example, the measurements of Young's modulus [50] on low-porosity bulk samples of nanocrystalline Cu and Pd showed only a small decrease from the value for coarse-grained samples. This decrease was attributed to the presence of residual

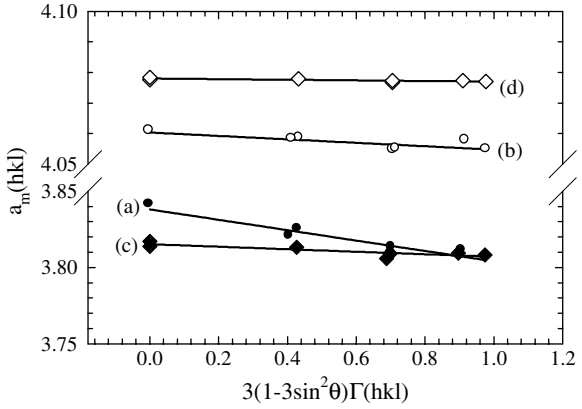

Figure 2. Typical gamma-plots. Labels (a)–(d) are the same as in figure 1. The error bars are much smaller than the symbol sizes.

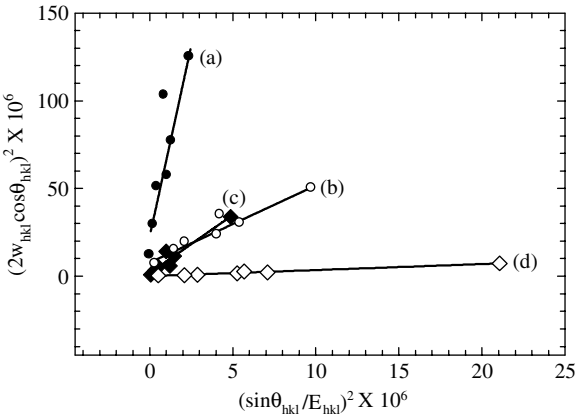

Figure 3. Typical $(2w_{hkl}\cos\theta_{hkl})^2$ versus $(\sin\theta_{hkl}/E_{hkl})^2$ plots. Labels (a)–(d) are the same as in figure 1. $2w_{hkl}$ is in radians. The error bars are smaller than the symbol sizes.

porosity in the samples. Further, the high-pressure x-ray diffraction measurements and the first-principles calculations [51] on nanocrystalline nickel showed no significant difference between the bulk moduli of nano-sized and large-grained nickel crystallites. Similar conclusions were drawn from the experiments on nanocrystalline (10 nm) iron samples [52]. Recent atomistic calculations of the elastic properties of metallic face-centered cubic nanocrystals [53, 54] show that the material length scale for elasticity is well below 10 nm, implying that the size effect on elasticity becomes important only for grain sizes below 10 nm. The line widths were analysed using equation (4). Figure 3 shows the typical plots resulting from equation (4). The d and $2p_{\max}$ were calculated from such plots.

Figure 4 shows the pressure dependence of d. Large errors in the estimations of d occur mainly because short-wavelength x-rays are used in the high-pressure diffraction experiments. The data are to 58.8 GPa for c-Au and to 55 GPa for n-Au. The trend line fitted to d versus pressure data suggests that the computed grain size in c-Au decreases from 120 ± 50 nm at ambient pressure (0.1 MPa) to 49 ± 10 nm at 60 GPa. The d in n-Au decreases from 33 ± 7 nm at 0.1 MPa to 9 ± 2 nm at 60 GPa. In both cases, the decrease in d under pressure is much

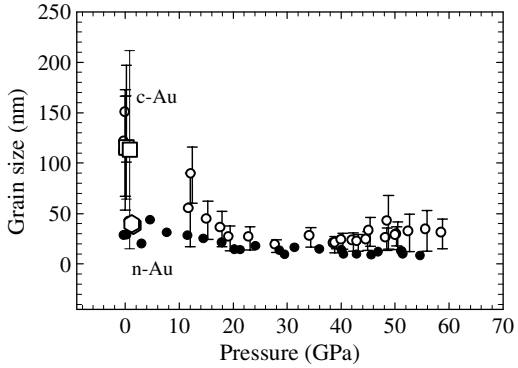

Figure 4. Variation of the crystallite size with pressure. Unfilled squares and hexagons indicate data on pressure release. For clarity, error bars on n-Au data are not shown. Error bars on either side equal the standard errors.

larger than the decrease expected solely from the compressibility of gold. For example, the compressibility of gold gives only a ≈6% decrease in d when pressure is increased from 0.1 MPa to 60 GPa. The measurements after decreasing the pressure from ≈60 to ≈1 GPa suggest that the observed grain-size reduction under pressure is reversible. The crystallites of a highly ductile gold are not expected to comminute during pressurization and, therefore, a permanent change in d is not expected. It is likely that localized stress gradients develop on compression and subdivide the crystallites into smaller coherently scattering domains that are interpreted from the line-width analysis as the grain size. Since the stress gradients relax on the release of pressure, the grain size reverts back to the initial value. A fuller explanation must await further studies of this nature. The observation of reversible grain-size reduction is not likely to be an artifact of the data analysis, because the same method of analysis gave a permanent grain-size reduction in MgO [40].

The pressure in the sample under nonhydrostatic compression develops a radial pressure gradient. The pressure gradients produce varying strain gradients in the sample. Since the primary beam has non-zero cross-sectional area (20 μm diameter in the present experiments), the diffraction pattern arises from the region of lattice-strain gradient. This causes the diffraction lines to broaden. This broadening arises due to the variations in lattice strain and will exhibit $\tan\theta$-dependence. Thus, the width from pressure gradients will contribute to micro-strains and consequently to $2p_{\max}$. A rigorous analysis of the effect of pressure gradients on the diffraction profiles can be carried out using the approach developed earlier [55]. Such an analysis is not possible in the present case, as many of the parameters required for the analysis were not measured in the present experiments. The possibility of axially symmetric pressure gradients causing a subdivision of the coherently scattered domains cannot be ruled out. In such a case, a contribution to the width varying as $1/\cos\theta$ will arise and affect the grain-size estimation.

The changes in the grain size arise from at least two distinct sources. The change due to the compressibility effect is the intrinsic material property and is small for most solids. The major change arises from the deformation of the sample during nonhydrostatic compression. The magnitude of the effect depends on the extent of deformation that the sample undergoes before a given pressure is established. The grains in brittle materials comminute on nonhydrostatic compression and the reduction in grain size is irreversible, while extremely ductile materials, like Au, appear to undergo reversible grain-size reduction. Application of truly hydrostatic

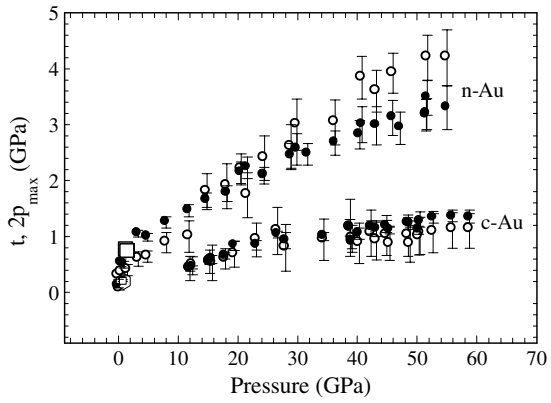

Figure 5. The pressure dependence of strength. The t and $2p_{max}$ are shown by unfilled and filled symbols, respectively. Unfilled squares and hexagons indicate data on pressure release.

pressure will produce negligible changes in the grain size and line widths. The results of diffraction experiments under hydrostatic pressure [56] support this conclusion. Thus, the measured grain size is not a unique function of pressure under nonhydrostatic compression.

Figure 5 shows the pressure dependences of t and $2p_{max}$. The two measures of strength give comparable results. The trend line through combined t and $2p_{max}$ versus pressure data suggest that the strength of c-Au increases from 0.12 ± 0.04 GPa at 0.1 MPa to 1.1 ± 0.12 GPa at 60 GPa. For n-Au, the strength increases from 0.4 ± 0.06 GPa at 0.1 MPa to 3.7 ± 0.4 GPa at 60 GPa. The strength decreases rapidly below 5 GPa for both c-Au and n-Au, and therefore the actual strength at 0.1 MPa is much lower than those calculated from the trend lines. The measurements after reducing the pressure from 60 GPa to $\approx$1 GPa suggest that the pressure dependence of strength is reversible.

The pressure enhancement of strength under nonhydrostatic compression arises from two distinct factors. One is the intrinsic pressure effect, which is present under truly hydrostatic pressure, and is related to the shear modulus increase under pressure. The second factor is grain-size strengthening. The form of the equation connecting strength with shear modulus and grain size depends on the grain size. For samples with grain sizes in excess of 1 μm, the deformation is controlled by the dislocation motion. In this grain-size range, the strength varies linearly with the shear modulus [57] and as $d^{-1/2}$ [58]. The grains in the range 1 μm–10 nm (a range relevant to this study) deform by grain-boundary shear promoted by the pile-up of dislocations that are restricted to their slip planes [58]. The strength still depends linearly on $d^{-1/2}$ with a positive slope. However, the dependence of strength on the shear modulus is no longer linear. The following relation for the pressure and grain-size dependences of strength can be derived from equation (19) of Conrad [58]:

$$2p_{max} = a_0 r(p) + a_1 [r(p)/d(p)]^{1/2}. \tag{5}$$

$2p_{max}$ is taken as a measure of strength. $r(p)$ is the ratio of the shear moduli at a pressure p and 0.1 MPa, and $d(p)$ is the pressure-dependent grain size;

$$a_0 = \alpha \mu_0 \mathbf{b} \rho_\mu^{1/2} \qquad \text{and} \tag{6}$$

$$a_1 = (\Delta F^*)^{1/2} \left(\frac{\mu_0 \mathbf{b}}{\pi v^*} \right)^{1/2}. \tag{7}$$

The symbols ρ_μ, $\mathbf{b}$, μ_0, v^*, and ΔF^* denote the dislocation density responsible for the long-range internal stress, Burger's vector, shear modulus at ambient pressure, activation

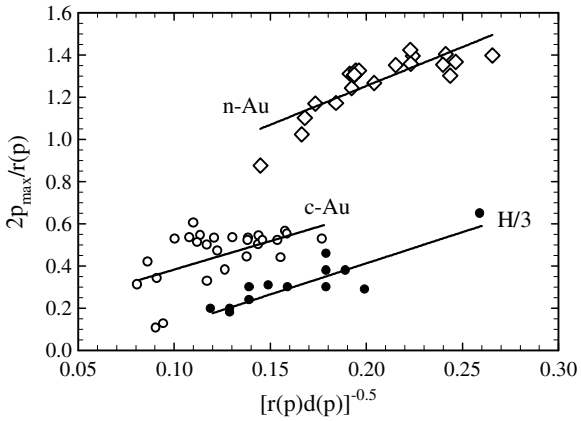

Figure 6. $2p_{\max}/r(p)$ as a function of $[r(p)d(p)]^{-1/2}$. Unfilled circles and diamonds indicate data for c-Au and n-Au, respectively. Filled circles show the strength derived from the grain size versus hardness data [42].

volume, and Helmlotz free activation energy, respectively. The symbol α (note the use of α with different meaning in equation (3)) is a constant that relates flow stress to the dislocation density. Since the present measurements are conducted at room temperature under static load, the strain-rate-dependent terms from a_1 are left out. The value of a_0 is expected to differ from sample to sample, since it contains dislocation density as one of the parameters. For this reason, it is difficult to compare the results of fitting equation (5) to the data from different samples. We first determined a_0 from the $2p_{\max}/r(p)$ versus $[r(p)d(p)]^{-1/2}$ plot shown in figure 6. Equation (5) suggests that the data set for each sample should lie on a straight line. The a_0-values, as determined from the intercepts of these plots, were 0.11 and 0.52 for c-Au and n-Au, respectively. An independent estimate of strength can be obtained from the hardness data. Many investigators (e.g. [50, 59]) have often used one third of the hardness as a measure of the yield stress. A detailed discussion of the relationship between hardness and strength can be found in many textbooks (e.g. [60]). The strength calculated from the hardness-grain-size data [42] are also shown in figure 6. Since these data are at ambient pressure, $r(p) = 1$. The a_0-value for this data set was -0.2. The strength data on c-Au, n-Au and those derived from the hardness measurements are compared in figure 7, which shows the $[2p_{\max} - a_0 r(p)]$ versus $[r(p)/d]^{1/2}$ plots. Equation (5) suggests that the data should lie on a straight line. It is seen that the data on samples from three different sources lie on a single straight line. The grain sizes of c-Au and n-Au are nearly equal at 30 GPa. If grain size and pressure determine the strength, then the strengths of the two samples should be equal at 30 GPa. Contrary to this expectation, figure 5 shows that the strength of n-Au is much higher. It may be noted that c-Au and n-Au samples are from two different sources and the micro-structural features are expected to be different, as these depend on the method of sample preparation. The differences in micro-structural features of the two samples are possibly reflected in very different a_0-values for c-Au and n-Au.

5. Conclusions

The grain size decreases significantly on compression of the sample in a diamond anvil cell. The reversibility of the grain size appears to be a feature of highly ductile materials and requires further investigation for a better understanding. In contrast, brittle materials show a permanent

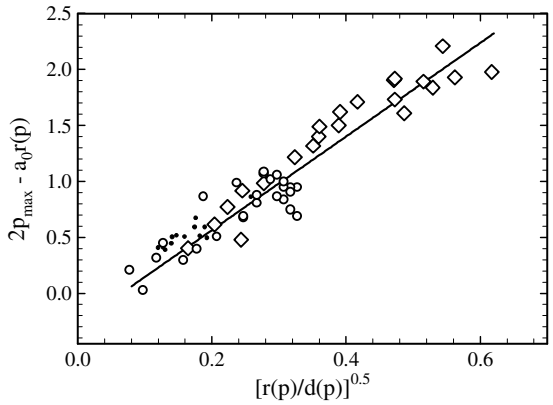

Figure 7. $[2p_{\max} - a_0 r(p)]$ as a function of $[r(p)/d]^{1/2}$. Unfilled circles and diamonds indicate data for c-Au (with $a_0 = 0.11$) and n-Au (with $a_0 = 0.52$), respectively. Filled circles (with $a_0 = -0.20$) show the strength derived from the grain size versus hardness data [42].

reduction in the grain size in the initial stages of compression. The compressive strength is a function of both pressure and grain size. The dislocation theory based equation relevant for grain sizes in the range 1 μm to 10 nm fits the present data well. The agreement between the strengths derived from the x-ray diffraction data and those from the hardness measurements indicate that t and $2p_{\max}$ are indeed measures of compressive strength. The grain-size effect on strength derived from the high-pressure diffraction data should be considered in a quantitative interpretation of the data.

Acknowledgments

We thank Y Meng and M Somayazulu for their technical assistance at HPCAT, Chicago. Nanomat Inc, Pa, USA gifted the well-characterized samples of nanocrystalline gold powder. SKS received financial support under the International Materials Institute project from the National Science Foundation (DMR 0231291) through Iowa State University (K Rajan). AKS thanks the director of the National Aerospace Laboratories for support.

References

[1] Ruoff A L 1975 *J. Appl. Phys.* **46** 1389
[2] Singh A K and Kennedy G C 1974 *J. Appl. Phys.* **45** 4686
[3] Singh A K 1993 *J. Appl. Phys.* **73** 4278
[4] Uchida T, Funamori N and Yagi T 1996 *J. Appl. Phys.* **80** 739
[5] Singh A K, Mao H K, Shu J and Hemley R J 1998 *Phys. Rev. Lett.* **80** 2157
[6] Singh A K, Balasingh C, Mao H K, Hemley R J and Shu J 1998 *J. Appl. Phys.* **83** 7567
[7] Haward C J and Kisi E H 1999 *J. Appl. Crystallogr.* **32** 624
[8] Singh A K and Takemura K 2001 *J. Appl. Phys.* **90** 3269
[9] Mathies S, Priesmeyer H G and Daymond M R 2001 *J. Appl. Crystallogr.* **34** 585
[10] Singh A K and Kennedy G C 1976 *J. Appl. Phys.* **47** 3337
[11] Kinsland G L and Bassett W A 1976 *Rev. Sci. Instrum.* **47** 130
[12] Kinsland G L and Bassett W A 1977 *J. Appl. Phys.* **48** 978
[13] Usha Devi S and Singh A K 1986 *Physica* B **138–140** 922
[14] Syassen K and Holzapfel W B 1978 *Rev. Sci. Instrum.* **49** 1107
[15] Jeanloz R, Godwal B K and Meade C 1991 *Nature* **349** 687

[16] Singh A K 1993 *Phil. Mag. Lett.* **67** 379
[17] Wu T-C and Bassett W A 1993 *Pure Appl. Geophys.* **141** 509
[18] Funamori N, Yagi T and Uchida T 1994 *J. Appl. Phys.* **75** 4327
[19] Hemley R J, Mao H K, Shen G, Badro J, Gllet P, Hanfland M and Häusermann D 1997 *Science* **276** 1242
[20] Kisi E H and Howard C J 1998 *J. Am. Ceram. Soc.* **81** 1682
[21] Mao H K, Shu J, Shen J, Hemley R J, Li B and Singh A K 1999 *Nature* **396** 741
[22] Duffy T S, Shen G, Shu J, Mao H K, Hemley R J and Singh A K 1999 *J. Appl. Phys.* **86** 6729
[23] Grima Gallardo P, Besson J M, Itié J P, Gauthier M, Mezouar M, Klotz S, Häusermann D and Hanfland M 2000 *Phys. Status Solidi* a **180** 427
[24] Ponkratz U, Nicula R, Jianu A and Burkel E 2000 *J. Phys.: Condens. Matter* **12** 8071
[25] Shieh S R and Duffy T S 2002 *Phys. Rev. Lett.* **89** 255507
[26] Merkel S, Wenk R H, Shu J, Shen G, Gillet P, Mao H K and Hemley R J 2002 *J. Geophys. Res.* **107** B11 2271
[27] Kavner A and Duffy T S 2003 *Phys. Rev.* B **68** 144101
[28] Singh A K 2004 *J. Phys. Chem. Solids* **65** 1589
[29] Merkel S, Shu J, Gillet P, Mao H K and Hemley R J 2005 *J. Geophys. Res.* **110** B05201
[30] Singh A K, Menéndez-Proupin E, Gutiérrez G, Akahama Y and Kawamura H 2006 *J. Phys. Chem. Solids* at press
[31] Stokes A R and Wilson A J C 1944 *Proc. Phys. Soc. (London)* **56** 174
[32] Langford J I 1971 *J. Appl. Crystallogr.* **4** 164
[33] Klug H P and Alexander L 1974 *X-ray Diffraction Procedures for Polycrystalline and Amorphous Materials* (Reading, MA: Addison-Wesley)
[34] de Keijser Th H, Langford J I, Mittemeijer E J and Vogels A B P 1982 *J. Appl. Crystallogr.* **15** 308
[35] Warren B E 1990 *X-Ray Diffraction* (New York: Dover)
[36] Singh A K, Vijayan K, Xia H, Vohra Y K and Ruoff A L 1992 *Recent Trends in High Pressure Research: Proc. 13th AIRAPT—Int. Conf. on High Pressure Science and Technology* ed A K Singh (New Delhi: Oxford IBH) pp 782–5
[37] Weidner D J, Wang Y and Vaughan M T 1994 *Science* **266** 419
[38] Chen J, Inoue T, Weidner D J, Wu Y and Vaughan M T 1998 *Geophys. Res. Lett.* **25** 1103
[39] Chen J, Weidner D J and Vaughan M T 2002 *Nature* **419** 824
[40] Singh A K, Liermann H P and Saxena S K 2004 *Solid State Commun.* **132** 795
[41] Chen J, Schmidt N, Chen J, Wang L, Weidner D, Zhang J and Wang Y 2005 *J. Mater. Sci. Lett.* **40** 5763
[42] Sakai S, Tanimoto H and Mizubayashi H 1999 *Acta Mater.* **47** 211
[43] Duffy T S, Shen G, Heinz D L, Ma Y, Shu J, Mao H K, Hemley R J and Singh A K 1999 *Phys. Rev.* **60** 15063
[44] Singh A K 2000 *Science and Technology of High Pressure (Proc. AIRAPT-17)* ed M H Manghanani, W J Nellis and M F Nicol (Hyderabad: Universities Press) p 62
[45] Singh A K, Jain A, Liermann P and Saxena S K 2006 *J. Phys. Chem. Solids* at press
[46] Chen J, Li L, Weidner D and Vaughan M 2004 *Phys. Earth Planet. Inter.* **143/144** 347
[47] Chen J *et al* 2006 *J. Phys.: Condens. Matter* **18** S1049
[48] Golding B, Moss S C and Averbach B L 1967 *Phys. Rev.* **158** 637
[49] Birch F J 1978 *J. Geophys. Res.* **83** 1257
[50] Sanders P G, Eastman J A and Weertman J R 1997 *Acta Mater.* **45** 4019
[51] Rekhi S, Saxena S K, Ahuja R, Johansson B and Hu J 2001 *J. Mater. Sci.* **36** 4719
[52] Chen B, Penwell D, Kruger M B, Yue A F and Fultz B 2001 *J. Appl. Phys.* **89** 4794
[53] Miller R E and Shenoy V B 2000 *Nanotechnology* **11** 139
[54] Shenoy V B 2005 *Phys. Rev.* B **71** 094104
[55] Singh A K 1992 *Recent Trends in High Pressure Research: Proc. 13th AIRAPT—Int. Conf. on High Pressure Science and Technology* ed A K Singh (New Delhi: Oxford IBH) pp 786–9
[56] Takemura K 2001 *J. Appl. Phys.* **89** 662
[57] Chua J O and Ruoff A L 1975 *J. Appl. Phys.* **46** 4659
[58] Conrad H 2004 *Metall. Mater. Trans.* A **35** 2681
[59] Jhi S-H, Loui S G, Cohen M L and Morris J W Jr 2001 *Phys. Rev. Lett.* **87** 075503
[60] Dieter G E 1988 *Mechanical Metallurgy SI Metric Edition* (New York: McGraw-Hill) pp 329–32